ALJEST

Enhancement of photocatalytic reduction of Cr(VI) using the hetero-system NiAl$_2$O$_4$/ZnO under visible light

R. Bouallouche[1-5], M. Kebir[2,3], N. Nasrallah[3,5*], M. Hachemi[1], A. Amrane[4], M. Trari[5]

[1]Faculty of Sciences Engineer, Research Unit Materials, Processes and Environment URMPE, University M'hamed Bougara of Boumerdes / FSI, Frantz Fanon City, Indépendance Avenue 35000 Boumerdes, Algeria.
[2]Research Unit on Analysis and Technological Development in Environment (URADTE CRAPC), BP 384, 42000 Bou-Ismail Tipaza. Algeria.
[3]Laboratory of Reaction Engineering, Faculty of Mechanical Engineering and Process Engineering USTHB, BP 32, 16111 Algiers, Algeria.
[4]Univ rennes, Ecole Nationale Supérieure de Chimie de Rennes, CNRS, ISCR – UMR6226, F15 35000 rennes, France
[5]Laboratory of Storage and Valorization of Renewable Energies Faculty of Chemistry USTHB, 17 BP 32, 16111 Algiers, Algeria.

*Corresponding author: nas_nour@yahoo.fr; Tel.: +213 00 00 00; Fax: +21300 00 00

ARTICLE INFO

ABSTRACT/RESUME

Abstract: *Hexavalent chromium Cr(VI) is well known to be a toxic and non-biodegradable contaminant and can cause significant environmental damage if it is not eliminate from wastewater. However, it can be reduced to Cr(III), which is less toxic by photocatalysis process using the heterosystem NiAl$_2$O$_4$/ZnO. NiAl$_2$O$_4$ prepared by nitrate method crystalize in a spinel structure and was characterized, by XRD, FTIR, and SEM techniques. NiAl$_2$O$_4$ acts as electrons pump and the electron transfer to chromate is mediated via ZnO. Under the optimized conditions, the percentage of Cr(VI) reduction was 62 % for 20 mg/L, NiAl$_2$O$_4$/ZnO ratio (1/1) at pH~3.7 and under visible light. An improvement up to 72% was obtained when the reaction occurs in a Rishton reactor with six bleds after 6 h illumination. It is therefore concluded that the Cr(VI) photocatalytic reduction followed a pseudo first order kinetic model, in agreement with the Langmuir–Hinshelwood mechanism. This work revealed that the NiAl$_2$O$_4$/ZnO heterosystem exhibits a better photocatalytic efficiency for the photoreduction of Cr(VI) mainly due to the good separation of electron-hole pairs (e-/h+) in this combination.*

I. Introduction

The available supplies of potable water is a real problem faced in the world [1]. Consequently, there has been a considerable pollution from industrial effluents and different of toxic substances (metals, pesticides, detergents, drugs, dyes etc...) are daily produced in large amounts and discharged in the aquatic medium without any restriction and control [2]. In this respect, a numerous works have been devoted to the water treatment by physical, chemical and biological processes [3]. Among the pollutants, heavy metals are non-biodegradable and accumulate progressively in living organisms, thus causing serious health problems [4- 6].

Chromium Cr(VI) exists in six oxidation states, the hexavalent is one of the most toxic valence found in various industrial activities which are the origin of the water contamination [7, 8] metal plating, tanning leather, electroplating, corrosion control, mining activities because of its properties, these activities represent the principal potential sources for generation of wastewaters. The increased of Cr(VI) concentration in the natural water causes a damage for bacteria, paralysis, eczema and carcinogenic effects [9]. These processes use a property of chromium (VI) making it a strongly oxidizing cation, but in the same makes it dangerous for both the health and environment.

The tolerance limit of Cr(VI) in domestic surface waters restricted by the organization WHO is limited at 0.1 mg/L and drinking water and 0.05 mg/L for the industrial wastewater [10]. In order to comply with this limit, it is essential that the industries treat their effluents to reduce the Cr(VI) concentration to reach the acceptable permissible levels before its spread into the natural environment.

Therefore, it has been a renewed interest in the techniques for its removal [11]. The conventional processes including ion exchange, membrane filtration, reverse osmosis, solvent extraction and coagulation are either expensive or difficult to use [12]. In addition, each technique has its own shortcomings and often does not comply with the threshold set up by the standards of WHO. The photoreduction appears a promising technology in the water treatment and environmentally friendly without adding chemical input or output and no residue is produced after operation treatment. Currently, it is used to catalyze the photo-induced degradation or the photoreduction of pollutants in air and water, odor control, bacterial inactivation, water splitting, hydrogen generation and the heavy metals reduction [13, 14].

In this context, catalysts having a small gap are more attractive for the exploitation of the solar energy [15] and the spinel-structured materials have attracted a large scientific attention because of their functional properties and the environmental cleanup. So, it turns out that the prospect of developing more efficient and durable systems becomes necessary. The photocatalysis has proved its usefulness in the water treatment [16, 17].

There are many researchers studied the Cr(VI) photoreduction onto oxides such as TiO_2, Nb_2O_5, MoS_2, CuS, ZnS [18]. The studies were extended to other catalysts like $BiVO_4$, $InSnS_2$, $ZnWO_4$ [14] and ZnO and heterosystems CdS/ZnAlO, $CuCo_2O_4/TiO_2$, $CuAl_2O_4/TiO_2$ [19, 20]. Among the candidates, $NiAl_2O_4$ has attracted a great interest because of its low cost and chemical stability [21]. The aim of our work is to study the photoreduction of the hazardous Cr(VI) using the $NiAl_2O_4/ZnO$ hetero-system under visible light, thereafter, optimizing the effects of the operating parameters.

The *n* type semiconducting ZnO provides a bridge between the conduction band of *p* type semiconductor $NiAl_2O_4$ and Cr(VI) ions. In addition, coupled semiconductors increase the charge separation by synergetic effect, extend the spectral response of ZnO to longer wavelengths, and inhibit the recombination rate of charge carriers. So, $NiAl_2O_4$ was prepared by chemical method, thus producing enhanced active surfaces than those obtained usually by solid-state reaction [22-25]. On the other hand, the effect of various parameters for the Cr(VI) reduction such as pH, initial Cr(VI) concentration and catalyst dose were studied under visible light irradiation.

II. Materials and methods

II.1. *Chemical reagents*

$Ni(NO_3)_2 6H_2O$ (Fluka,99%), $Al(NO_3)_3$ $6H_2O$ (Aldrich 99%); HNO_3(Merck, 69%) and all other reagents and solvents for syntheses were purchased from commercial sources and used without further purification. NaOH and H_2SO_4 solutions were used for pH adjustment.

II.2. Catalyst synthesis

In a molar ratio (½) the spinel $NiAl_2O_4$ was prepared by decomposition of metal nitrates [21], were used as starting reagents. Solution containing 1 mol of $Ni(NO_3)_2$ $6H_2O$ and 2 mol of $Al(NO_3)_3$ $6H_2O$ were dissolved in distilled water with a minimum of HNO_3 (69%). The mixture was stirred and slowly heated to preclude ejection in a ventilated place. Water and NO_x fumes were progressively removed by heating. The bluish green powder was homogenized in an agate mortar and heated at 850 °C for 20 h with intermediate regrinding.

II.3 Characterization

The thermal gravimetric (TGA) and differential thermal analysis (DTA) were performed on TEA SDTQ 600 instrument up to 1100 °C at a heating rate of 10 °C min^{-1} under air. The crystalline structure was elucidated by X-ray diffraction using a Bruker D8 X-ray diffractometer (XRD), using Cu Kα radiation (λ= 1.54178 A). The data were collected over the range (5 - 90°) in steps of 5° (2θ) min^{-1}; the patterns were indexed according to JCPDS Card N°. 10-0339. The morphology of the surface micro structure of spinel was investigated by a Quanta TM 250 FEG scanning electron microscope (SEM). The determination of the size distribution was performed on the powder by a laser size analysis (Mastersizer 2000 ver. 2.00, Malvern Instruments Ltd).

The Fourier transform infrared (FTIR-ATR) and UV-Vis diffuse-reflectance spectroscopy were recorded with a Bruker Optics Alpha one instrument and Jasco 650 UV-Visible spectrophotometer equipped with integrated sphere, respectively.

ALJEST

II.4 Photocatalytic measurement

The stock solution (1000 mg/L) was prepared by dissolving $K_2Cr_2O_7$ (Merck, 99.5%) in distilled water. The catalyst dose was fixed at 1 g ƒ((1−x) $NiAl_2O_4$/x ZnO)ƒ L^{-1}. The adsorption tests were carried out in a laboratory-scale double walled reactor. The powder with a known Cr(VI) concentration was placed in the reactor and the mixture was homogeneously dispersed by magnetic stirring. The temperature was controlled thanks to a thermostated bath (Julabo). The pH was adjusted by H_2SO_4 and NaOH and monitored by a pH-meter (Hanna pH211). The experiments were conducted under illumination of a tungsten lamp (200 W); the radiant flux was measured with a commercial radiometer (Testo 545) and may be varied by moving the lamp closer to or farther from the reactor. The aliquots were removed at regular times for the analysis of the Cr(VI) concentration. The solution was then filtrated on a Wattman filter paper in order to separate the grains from the solution and systematically acidified by H_2SO_4. Cr(VI) was complexed with 1,5-diphenylcarbazide and the absorbance was measured at 540 nm [19]. The Cr(VI) concentration was determined by spectrophotometry with a double beam UV-Visible spectrophotometer (UV-1800, Shimadzu, Nakagyo-ku, Kyoto, Japan) using quartz cell with 1 cm path length. The titrations were performed in triplicate and the mean values were reported.

A blank reaction without catalyst as control was also carried out under the same conditions. The removal efficiency (R%) and the adsorption capacity (q_e) of Cr(VI) onto the heterosystem $NiAl_2O_4$/ZnO were calculated from the initial concentrations (C_o), (C_t) at time (t), and equilibrium (C_e):

$$R\ (\%) = \frac{(C_o - C_t)}{C_o} * 100 \qquad \qquad \textbf{(1)}$$

$$qe = \frac{V(C_o - C_e)}{m} * 100 \qquad \qquad \textbf{(2)}$$

Where, V is the volume of the solution (L) and m is the mass of the $NiAl_2O_4$/ZnO(g).
The adsorbed amount q_e (mg g^{-1}) was determined from the mass balance.

III. Result and discussion

III.1. Characterization of $NiAl_2O_4$

The TGA plot of $NiAl_2O_4$ is shown in Figure.1, the initial evolution of temperature of the nitrate vapors is 400 °C. The maximum calcined temperature of $NiAl_2O_4$ semiconductor is found to be 1000 °C. At this temperature, all nitrates were completely decomposed.
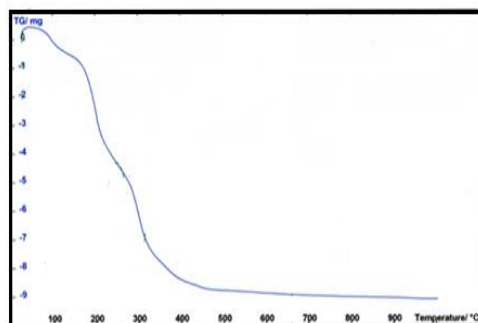

Figure 1. *TGA plot of the nitrate mixture used for NiAl₂O₄ preparation under air atmosphere.*

Figure. 1 shows the thermal behavior of the precursor before calcination. Two mass losses occurred; first, the weight mass losses in the range (25- 250 °C), is attributed to the elimination of physically adsorbed water and the beginning decomposition of nitrates. The second stage (250 and 500 °C) is due to the decomposition of nitrates. Nevertheless, small weight loss was observed above 500 to 1000 °C. According to the TGA analysis the crystallite phase should be obtained at 850 °C.
The XRD pattern of $NiAl_2O_4$ (Figure. 2) confirms the formation of the spinel structure in agreement with the JCPDS (PDF10- 0339). At 850 °C, the spinel exhibits a bluish green color and the main (hkl) reflection are 220, 311, 400, 420, 511, 440, 620 and 533. The narrow peak reveals single phase purity of $NiAl_2O_4$ and a better crystallinity (Figure. 2).
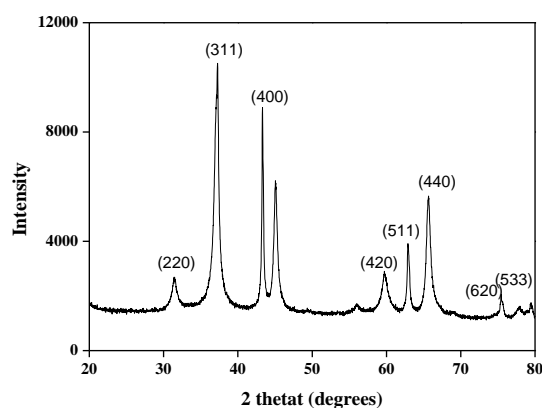

Figure 2. *XRD patterns of the spinel NiAl₂O₄ synthesized by nitrate route.*

The specific surface area **0.7198** m²/g and pore volume 20.61 µm were obtained from nitrogen adsorption isotherms at 77 K using a surface area analyzer (ASAP 2010 Micromeritics apparatus). The spinel has an optical gap of 1.72 eV, well suitable for the solar spectrum and exhibits a moderate conductivity with *p*-type conduction (data not shown).

The FT-IR spectra of the spinel NiAl$_2$O$_4$ was illustrated in Figure. 3. FTIR spectra of sample is show characteristic vibrational peaks of the spinel phase in the range (500-900 cm^{-1}) which can be attributed to vibrations of metal-O, Al-O, and metal-O-Al bonds [26].

NiAl$_2$O$_4$ is a normal spinel and the high frequencies peaks (715, 490 and 417 cm^{-1}) are assigned to stretching vibrations of Al-O and Ni-O bonds in both octahedral and tetrahedral sites (Ni^{+2}, Al^{3+}) confirming the formation of single phase NiAl$_2$O$_4$. The spectrum looks similar to that given in the recent literature [27].
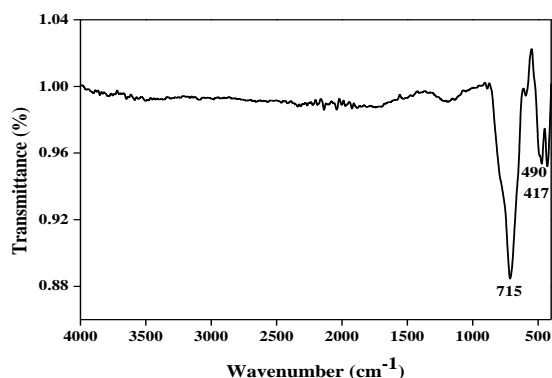

Figure 3. *The FTIR spectrum of the spinel NiAl$_2$O$_4$ elaborated at 900 °C.*
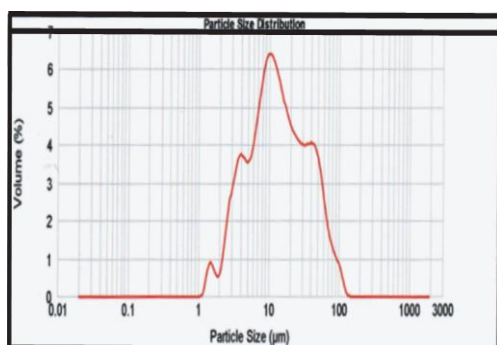

Figure 4. *The particle size distribution of the spinel NiAl$_2$O$_4$.*

Figure. 4 shows that there was a broader distribution in the oxide particles; it consists of agglomerated polycrystals, and which disintegrates during hot-pressing. Based on the above, it is suggested that, the powder agglomeration leads to in homogeneous composites and variations in packing density, after hot-pressing. This statement implies that strength impairment as a result of containing large agglomerated particles of spinel. The mean particle size distribution analysis of NiAl$_2$O$_4$ powder is found to be 10 µm (Figure. 4).

The surface morphology of the spinel was investigated by high resolution scanning electron microscopy. The SEM images of NiAl$_2$O$_4$ prepared by nitrate method (Figure. 5) could infer that the NiAl$_2$O$_4$ nanoparticles were formed.
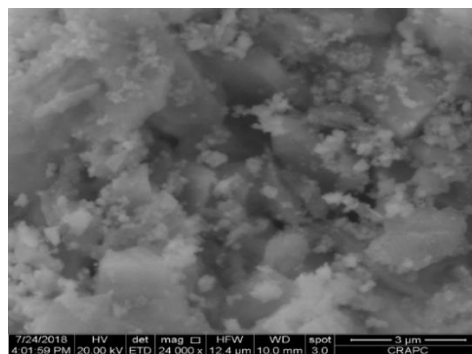

Figure 5. *SEM micrograph of NiAl$_2$O$_4$ prepared at 850 °C.*

The micrograph reveals a particle agglomerates (non dense) with a large distribution with a large pores and holes in their structure. It also reveals a similar morphology of widely distributed soft particle agglomerates, which is likely due to the large amount of gas released during combustion. However, the micrograph shows a weak porosity of NiAl$_2$O$_4$ but such value is slightly under estimated.

III.2. Adsorption equilibrium tests

A preliminary adsorption in the dark of Cr(VI) onto the heterosystem NiAl$_2$O$_4$ /ZnO was carried out in order to evaluate the adsorption capacity and to distinguish between the adsorption and photoreduction phenomena. 100 ml of Cr (VI) at a concentration of 20 mg/L was stirred in the presence of NiAl$_2$O$_4$/ZnO (0.05 g/0.05 g) for 3 h at a 25 °C. Figure 6 shows the variation of the Cr (VI) concentration as a function of time in the presence of the heterosystem made it possible in the first place to verify that the adsorption equilibrium is reached after 1 h. It is found that the reduction is important at the beginning of the experiment the initial concentration in the solution was reduced after 60 min; this results from the dark adsorption.

The difference between the nominal concentration and that measured after equilibrium is taken as the quantity of adsorbed Cr(VI) and a value of 8.75 % removal efficiency has been found. So, it is tempting to conclude that the Cr(VI) reduction is partially due to the dark adsorption which promotes the photocatalytic process (see below).
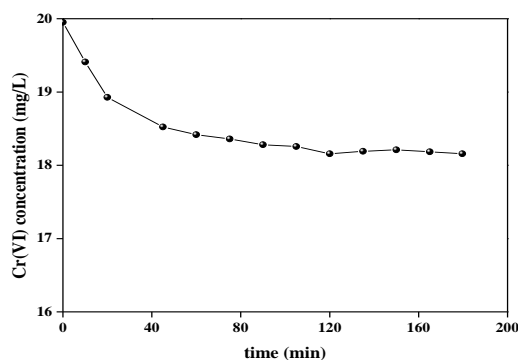
A LJEST

Figure 6. *The evolution of the Cr(VI) concentration by adsorption in the dark onto the heterosystem NiAl$_2$O$_4$ /ZnO as a function of time, ([Cr(VI)]$_o$= 20 mg/L, 0.05 g of ZnO, 0.05 g of NiAl$_2$O$_4$, 25 °C and pH =5.8).*

III.3. Photoreduction study of Cr(VI)

Prior to irradiation studies, the powders suspension were stirred in solution in the dark for 2 h to ensure the adsorption equilibrium. The zero-time reading was obtained from the blank solution kept in the dark. After a specific time of irradiation, the sample was withdrawn for the analysis of Cr(VI). The photocatalytic reduction was monitored by UV-Visible spectrophotometry.

III.3.1. Effect of contact time

The kinetic of Cr(VI) photoreduction was carried out to determine the required time for all experiments at a 25 °C. A mass of 0.1 g of heterosystem 50%NiAl$_2$O$_4$/50%ZnO was added to 100 mL of Cr(VI) solution at t = 0 min. The kinetic studies was conducted in a batch reactor. Samples are taken at regular time then filtered and analyzed. The experiment was stopped when the equilibrium is reached. Figure 7. Represents the variation in Cr(VI) concentration as a function of time.
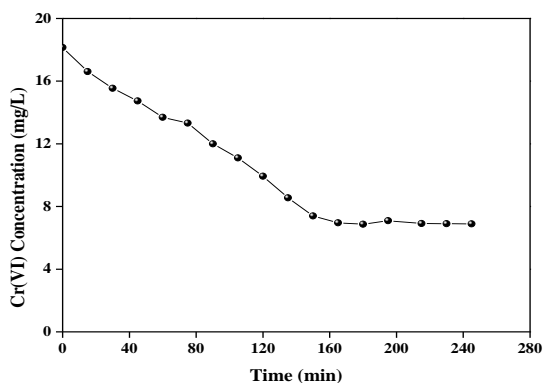

Figure 7. *The evolution of the Cr(VI) photoreduction as a function of time. ([Cr(VI)]= 20 mg/L, 0.05 g of ZnO, 0.05 g of NiAl$_2$O$_4$, at 25 °C and illumination (200 W)).*
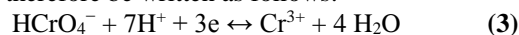
In this part, as presented in Figure 7, the illumination of Cr(VI) by visible light in presence of the heterosystem NiAl$_2$O$_4$/ZnO shows that there is a steady decrease in the concentration of Cr(VI) with irradiation time, 62,24 % of Cr(VI) was reduced to Cr(III) after 3 h. Afterward, the Cr(VI) remain nearly constant.

III.3.2. Effect of pH

The pH is crucial for optimizing the operating conditions of the photoreduction process. An experiments have been performed at 25 °C by varying the pH of Cr(VI) solution in the range (3.7 - 8) by adding of H$_2$SO$_4$ or NaOH 0.1 M. while keeping the others parameters constant such as the initial concentration and catalyst dose. The effect of pH on the photoreduction efficiency of Cr(VI) is presented in Figure. 8.

The rate of Cr(VI) photoreduction was found to be pH dependent, at acidic pH a maximal removal efficiency is obtained at pH = 3.7. Above this value the yield decreases sharply to 10 % as the pH value increases to 8. Then, HCrO$_4^-$ is predominant than Cr$_2$O$_7^{2-}$ H$_2$CrO$_4^0$, HCrO$_4^-$, CrO$_4^{2-}$ and Cr$_2$O$_7^{2-}$in the pH range studied (pH = 3.7). The semiconductor induces the appearance of positive charges on the surface which implies an adsorption of HCrO$_4^-$. Thus behavior can be explained by the electrostatic repulsion between negative Cr(VI) species and negatively charged NiAl$_2$O$_4$/ZnO heterosystem increased with increasing pH, and thereby resulting in the decreased reduction of Cr(VI) [28]. The surface catalyst is positively charged and shows an affinity with the chromate ions. The difference between the nominal concentration and that measured after equilibrium is taken as the quantity of adsorbed HCrO$_4^-$ and a value of 23% has been found. So, it is tempting to conclude that the Cr(VI) reduction is due to the dark adsorption which promotes the photocatalytic process (62 %). The global reduction reaction of HCrO$_4^-$ at pH =3 can therefore be written as follows:

$$HCrO_4^- + 7H^+ + 3e \leftrightarrow Cr^{3+} + 4\,H_2O \qquad \textbf{(3)}$$

As mentioned above, the main merit of the spinel is in the invariance of electronic bands with pH. This would allow an adjustment of NiAl$_2$O$_4$-CB with respect to ZnO-CB, the latter varies by 0.059 V decade^{-1}. Besides, the photocatalytic performance of ZnO is hampered by the large gap ($\sim$ 3.2 eV) which has showed no activity over 4 h illumination period. The hetero-systems allow the extension of the spectral photoresponse of ZnO toward the visible region where NiAl$_2$O$_4$ works as an electron pump. Thereafter, the straightforward explanation of the enhanced activity is that the electrons migrate to HCrO$_4^-$ via ZnO interfacial mechanism reaction. The Cr(VI) reduction onto the *p*-NiAl$_2$O$_4$/*n*-ZnO junction is thermodynamically feasible but requires a large over-potential and light can be used in this purpose:
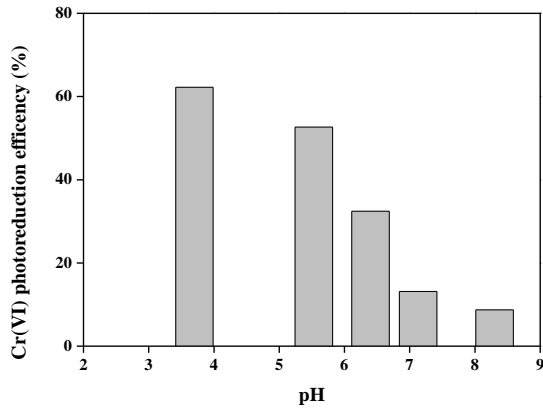
Figure 8. The evolution of the Cr(VI) photoreduction as a function of pH. ([Cr(VI)]= 20 mg/L, 0.05 g of ZnO, 0.05 g of NiAl₂O₄, 25 °C, 3 h, 350 rpm, illumination (200 W)).
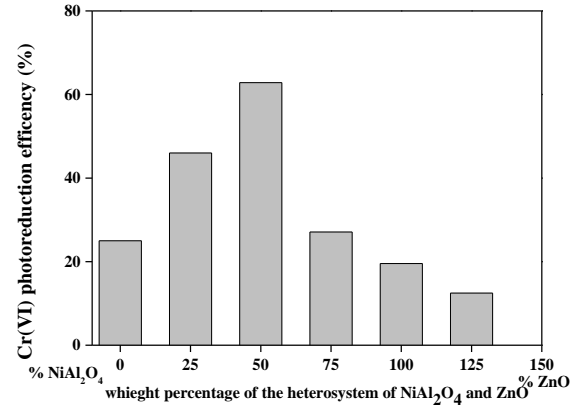

Figure 9. The evolution of the Cr(VI) photoreduction as a function of ratio (NiAl₂O₄/ZnO) ([Cr(VI)]= 20 mg/L, 25 °C, 350 rpm, 3 h, pH= 3.7 and illumination (200 W).

III.3.3. Effect of the percentage of heterojunction

The photoreduction of Cr(VI) to Cr(III) for different percentages weight of the heterosystem (x)% NiAl$_2$O$_4$ and (1-x) % ZnO was investigated under visible light. The influence of percentage weight of NiAl$_2$O$_4$ and ZnO (mg catalysts/mL solution) for total mass of catalysts 1 g/L on the photoactivity is illustrated in Figure. 9. The histogram gives a significant increase up to a liquid solid ratio equal to 1. This is explained by the increased of the active sites of NiAl$_2$O$_4$ /ZnO, and consequently an improvement of the photoactivity. In addition, other factors may be considered when the amount of catalyst increases like the optical effect of screen and / or increased light scattering by the particles. It is important to outline that the charges transfer takes place when the two semiconductors are in contact and that the increase in the catalyst concentration increases the collision probability of particles. This remains valid up to a critical concentration value of 50%/50% which exhibits the best photo-reduction efficiency (62%) due to the effective separation of charge carriers. Moreover, by using electron and hole scavengers, they concluded that the OH* radicals are the main active species for the Cr(VI) photoreduction. Yang et al. [29] produced ZnO nanofibers decorated with β-Bi$_2$O$_3$ nanoparticles and showed improved photoreduction of Cr(VI) under visible light.

III.3.4. Effect of the initial Cr(VI) concentration

The dependence of the rate photocatalytic activity on the initial Cr(VI) concentrations C$_o$ is an important point both from mechanistic and application [30]. The effect of Cr(VI) concentration was evaluated in the range (10-50 mg/L) at pH 3.7, 25 °C under visible light.

With increasing C$_o$ in initial Cr(VI) concentration, the residual concentration of Cr(VI) increases from 1 to 9 mg/L after photoreduction for 10 to 50 mg/L initial Cr(VI) concentration. However, most Cr(VI) could also be removed by the subsequent photoreduction (99%) for 10 mg/L initial concentration. In addition, the results clearly show that both the reduction and the rate decrease with increasing C$_o$ and an optimal value is obtained for 20 mg/L where the complete reduction occurs in less than 3 h (Figure. 10). Therefore, the number of accessible photocatalytic sites is simular than the Cr(VI) ions at low concentrations and the photoactivity increases with increasing C$_o$ until the saturation of the catalytic sites by Cr(VI) ions.
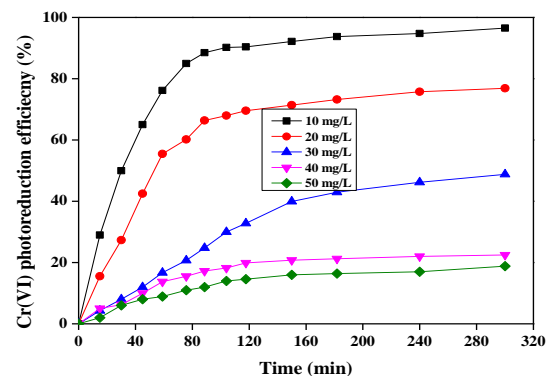

Figure 10. The evolution of the Cr(VI) photoreduction as a function of initial concentration, (NiAl₂O₄/ZnO= 50/50 , 25 °C, 350 rpm, 3 h, pH= 3.7 and illumination (200 W)).

III.3.5. Influence of the agitation rate and number of blades on the Cr(VI) photoreduction

In order to show the influence of the stirring geometry on the photocatalytic activity, we used three different types of Rushton type impellers with three blades (marine propellers), 3, 4 and 6 blades from 20 mg/L of Cr(VI). This study made it possible to highlight the effectiveness of agitation mobile and its optimal geometry [11]. The operating conditions are maintained fixed as previously (Figure 11):
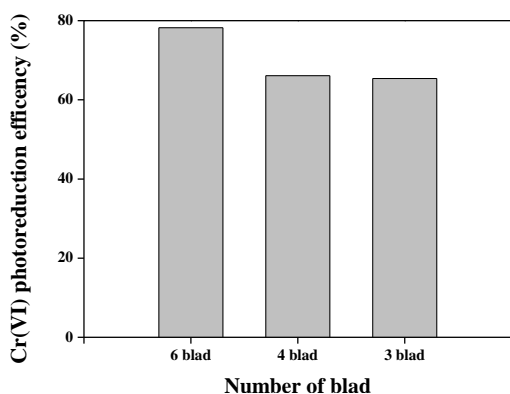
Figure 11. *Influence of impeller type and number of blades (b) on the Cr(VI) photoreduction. (NiAl$_2$O$_4$/ZnO = 50/50, 25 °C, 350 rpm, 3 h, pH= 3.7 ander illumination (200 W)).*

Figure.11. shows that the conversion yield increases up to 78 % when the reaction is carried out in a double walled stirred reactor. The reactor works with Rushton type impellers having six straight blades delivering essentially radial flow under an agitation speed of 350 rpm above which the photo-activity remain constant (Figure. 11).

III.4. Adsorption isotherms study

The equilibrium isotherm represents the relationship and the interaction between the concentration of the Cr(VI) adsorbate in solution and the Cr(VI) amount adsorbed in the dark. To evaluate this, various models were applied, such as Freundlich and the Langmuir isotherm, to define the equilibrium features of adsorption [31].

The Cr(VI) adsorption equilibrium is reached within 120 min of contact time under magnetically stirred Cr(VI) solutions, in the dark, on the surface of NiAl$_2$O$_4$/ZnO is shown in Figure. 6. The Langmuir adsorption isotherm is represented by the following equation:

$$\frac{Ce}{qe} = \frac{Ce}{qo} + \frac{1}{bqo} \qquad (4)$$

where C_e (mg L^{-1}) is the equilibrium Cr(VI) concentration, q_e and q_o (mg g^{-1}) are the adsorbed amounts at equilibrium and maximal capacity, and b (L mg^{-1}) the Langmuir constant (Figure. 12).

The Freundlich isotherm valid for the description of multilayer adsorption is represented by the following equation [32]:

$$Ln(qe) = Ln(kf) + \left(\frac{1}{n}\right)\left(Ln(Ce)\right) \qquad (5)$$

K_f and $1/n$ are constants related to the adsorption capacity and adsorption intensity, respectively. The parameters of the isotherms model are reported in Table 1.
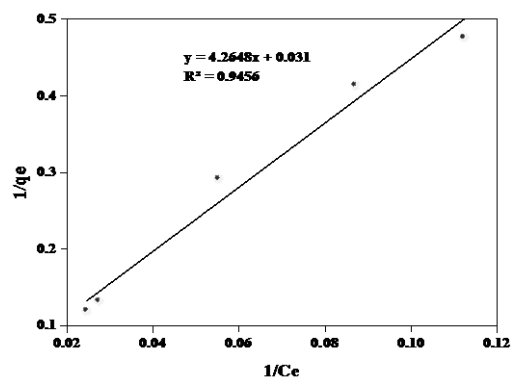
Figure 12. *Linearization of the Langmuir model for the adsorption of Cr(VI).*
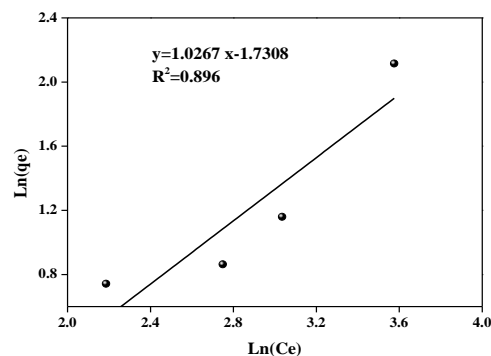
Figure 13. *Linearization of the Freundlich model for the adsorption of Cr(VI).*

Table 1. Parameter isotherm models for the adsorption of Cr (VI)

Langmuir model			Freundlich model		
A **(mg.g^{-1})**	**b** **(L.mg^{-1})**	**R^2**	**n**	**K_f**	**R^2**
4.2648	0.031	0.9456	1.0267	5.6406	0.896

By adjusting the experimental points on both models, and based on the values of the coefficient R^2, it appears that the isotherm of Langmuir model (Figure 12.) fit well the type of adsorption ($R^2 = 0.9456$). Thus, Cr(VI) could be adsorbed into monolayers on NiAl$_2$O$_4$/ZnO.

III.5. Kinetics of the Cr(VI) photoreduction

The kinetics of Cr(VI) reduction under visible light are analyzed using pseudo first order and pseudo

second order. The surface adsorption has a direct effect on the photoactivity, on the increasing number of photocatalytic sites.

The apparent pseudo first order equation is expressed by:

$$r = -\frac{dC}{dt} = k_{app} \, C_o \qquad (6)$$

Where,

r: is the rate and k_{app} (mn^{-1}) the apparent pseudo first order rate constant. The integrated linear form of the pseudo first order model is presented as follows:

$$\ln\frac{Co}{C} = k_{app} \, t \qquad (7)$$

Where, C_o is initial Cr(VI) concentration; k_{app} (min^{-1}) the pseudo first order rate constant. The plot of $\ln(C_o/C)$ versus *t* gives in a linear relationship from which kapp was determined from the slope of the graph (Figure. 14). The kinetic parameters and R^2 value of the pseudo first order rate equation are shown in Table 2. The linear plot of ln C_o/C vs time *t*. illumination time shows that the reduction follows a pseudo first order.

Table 2. Pseudo-first-order kinetics constants, correlation coefficients (R^2) and half life time at different initial concentrations of Cr(VI).

C_o (mol/L) $\times 10^4$	R^2	k_{app}	$t_{1/2}$ (min)
1.9234	0.9952	0.024	28.875
3.8468	0.972	0.014	49.5
5.7703	0.983	0.011	63
7.6937	0.999	0.009	77
9.6172	0.982	0.003	231

The line indicates an apparent kinetics of Cr (VI) reduction is of pseudo first order. Thus, based on the coefficients R^2, it turns out that it is the pseudo first order model which best describes the photoreduction phenomenon of Cr(VI).

The Cr(VI) reduction is described by a pseudo firs order kinetic, which is rationalized in terms of the modified Langmuir–Hinshelwood (L–H) model, to accommodate the reactions occurring at a solid–liquid interface [33]. Whose rate is expressed by the following equation:

$$\frac{1}{k_{app}} = \frac{1}{k_r k_s} + \frac{C_o}{k_r} \qquad (8)$$

the rate constant k_r and adsorption coefficient k_s were found to be 0.011 mol/min L and 57.187 L/mol.
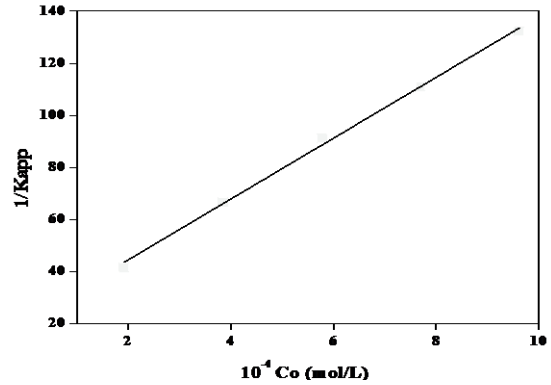

Figure 14. *The plot of $1/k_{app}$ versus Cr(VI) initial concentration C_o.*

The slope and the intercept of the linear plot of $1/k_{app}$ against C_o (Figure. 14) give the constants kr (0.893 mg L^{-1} min^{-1}) and ks (0.052 L mg^{-1}).

IV. Conclusion

The work was focused on the photoreduction of Cr(VI) on the $NiAl_2O_4$/ZnO heterosystem under visible light, $NiAl_2O_4$ was prepared by a facile nitrate route. The morphology of the spinel was characterized by SEM and XRD and FTIR techniques. Through the photoreduction experiments using aqueous Cr(VI) solution as a target contaminant, we found that the newly $NiAl_2O_4$/ZnO exhibited higher photo-catalytic efficiencies than pure ZnO or $NiAl_2O_4$ under visible light.

The results showed that the as-prepared $NiAl_2O_4$/ZnO exhibit a high photocatalytic activity and stability in the photoreduction of Cr(VI). The electronic coupling between the two materials and the high specific surface area contributed to the superior photocatalytic activity. $NiAl_2O_4$/ZnO composite was a potential photocatalyst for Cr(VI) reduction.

The rate of Cr(VI) photoreduction on $NiAl_2O_4$/ZnO was found to be pH-dependent. The decrease of the Cr(VI) concentration during irradiation was described by a first-order kinetic. The dependence of the reaction rate on the initial concentration of the probe molecule in the aqueous phase was described by a Langmuir–Hinshelwood model. However, the Langmuir adsorption constants determined from the adsorption isotherms of Cr(VI) in the dark are smaller than the adsorption constant determined from the analysis of the Langmuir–Hinshelwood type kinetics of the photocatalytic activity of the probe molecule. Under the experimental conditions, the photoreduction rates were higher than the rate of the adsorption of Cr(VI) in the dark. This finding reported here can be extended to other heterosystem material systems for environmental applications.

V. References

1. Susana Torres, L.; Maria de los Angeles, B.; Beatriz Rodríguez, L. Water accounts in decision-making processes of urban water management: Benefits, limitations and implications in a real implementation. *Sustainable cities and society* 50(2019) 101676.

2. Frank Spellman, R. Water & Wastewater Infrastructure: Energy Efficiency and Sustainability, *CRC Press* (2013) by Taylor and Francis group.

3. Marie, E.; Ludovic. Dumée, F.; Judy, L. Nano/microplastics in water and wastewater treatment processes-Origin, impact and potential solutions. *Water Research* (2019) 621-638.

4. Lee. S.Y.; Park, S.J. TiO_2 photocatalyst for water treatment application. *Journal of Industrial Engineering and Chemistry* 19 (2013) 1761-1769.

5. Rahman, A.; Jayaganthan, R. Study of photocatalyst magnesium aluminate spinel nanoparticles. *Journal of Nanostructure and Chemistry* 5 (2015) 147-151.

6. Liang, R.; Jing, F., Shen, L.; Qin, N.; Wu, L. MIL-53(Fe) as a highly efficient bifunctional photocatalyst for the simultaneous reduction of Cr(VI) and oxidation of dyes. *Journal of Hazardous Material* 287 (2015) 364-372.

7. Long, Z.; Fenglian, F.; Bing, T. Adsorption and redox conversion behaviors of Cr(VI) on goethite/carbon microspheres and akaganeite/carbon microspheres composites. *Chemical Engineering Journal* 356 (2019) 151-160.

8. Ying, H.; Qiang, X.; Jie, T.; Xin, F.; Honghan, C. New insights on Cr(VI) retention by ferrihydrite in the presence of Fe(II). *Chemosphere* 222(2019) 511-516.

9. Kebir, M.; Chabani, M.; Nasrallah, N.; Bensmaili, A.; Trari, M.; Coupling adsorption with photocatalysis process for the Cr(VI) removal. *Desalination* (270) 1-3, 1 (2011) 166-173.

10. Avner, V.; Rachel, C.; Jonathan, K.; Jennifer, H.; S, K. Andrew J, R. Laura S, M. Rose B., D. Gary S, Origin of Hexavalent Chromium in Drinking Water Wells from the Piedmont Aquifers of North Carolina. *Environmental Science Technology Letter* 312 (2016) 409-414.

11. Nasrallah, N.; Kebir, M.; Koudri, Z.; Trari, M. Photocatalytic reduction of Cr(VI) on the novel hetero-system $CuFe_2O_4$/CdS. *Journal of Hazardous Materials* 185, 2-3, (2011) 1398-1404.

12. Yu Zhang Miao, L.; Jiacheng, L.; Yanyan, Y.; Xiang, L. Surface modified leaves with high efficiency for the removal of aqueous Cr(VI). *Applied Surface Science* 484 (2019) 189-196.

13. Yang, L.; Xiao, Y.; Liu, S.; Li, Y.; Cai, Q.; Luo, Sh. Guangming Zeng, Photocatalytic reduction of Cr(VI) on WO_3 doped long TiO_2 nanotube arrays in the presence of citric acid. *Applied Catalysis. B Environment* 94 (2010) 142-149.

14. Sun, J.; Mao, J.-D.; Gong, H.; Lan, Y. Fe(III) photocatalytic reduction of Cr(VI) by low-molecular-weight organic acids with -OH. *Journal of Hazardous Materials* 168 (2009) 1569-1574.

15. Wang, N.; Xu, Y.; Zhu, L.; Shen, X.; Tang, H. Reconsideration to the deactivation of TiO_2 catalyst during simultaneous photocatalytic reduction of Cr(VI) and oxidation of salicylic acid. *Journal of Photochemistry and Photobiology. A: Chemistry* 201 (2009) 121-127.

16. Wang, L.; Wang, N.; Zhu, L.; Yu, H.; Tang, H. Photocatalytic reduction of Cr(VI) over different TiO_2 photocatalysts and the effects of dissolved organic species. *Journal of Hazardous Materials* 152 (2008) 93-99.

17. Xie, B.; Zhang, H.; Cai, P.; Qiu, R.; Xiong, Y. Simultaneous photocatalytic reduction of Cr(VI) and oxidation of phenol over monoclinic $BiVO_4$ under visible light irradiation. *Chemosphere* 63 (2006) 956-963.

18. Alias, N.; Rosli, S. A.; Hussain, Z.; Kian, T. W.; Lockman, Z. Anodised porous Nb_2O_5 for photoreduction of Cr(VI). *Materials Today: Proceedings,* 17, *Part* 3(2019) 1033-1039.

19. Kebir, M.; Trari, M.; Maachi, R.; Nasrallah, N.; Bellal, B.; Amrane, A. Relevance of a hybrid process coupling adsorption and visible light photocatalysis involving a new hetero-system $CuCo_2O_4$/TiO_2 for the removal of hexavalent chromium. *Journal of Environmental Chemical Engineering* 3, 1 (2015) 548-559.

20. Chakrabarti, S.; Chaudhuri, B.; Bhattacharjee, S.; Ray, A.K.; Dutta, B.K. Photoreduction of hexavalent chromium in aqueous solution in the presence of zinc oxide as semiconductor catalyst. *Chemical Engineering Journal* 153 (2009) 86-93.

21. Sebai, I.; Salhi, N.; Rekhila, G.; Trari, M. Visible light induced H_2 evolution on the spinel $NiAl_2O_4$ prepared by nitrate route. *International Journal of hydrogen energy* 42 (2017) 26652-26658.

22. Kabra, K.; Chaudhary, R.; Sawh ney R, L. Solar photocatalytic removal of Cu(II), Ni(II), Zn(II) and Pb(II): speciation modeling of metal-citric acid complexes. *Journal of Hazardous Materials* 155(2008) 424-432.

23. Kalai Selvan, R.; Augustin, C.O.; Sanjeeviraja, C.; Pol, V.G.; Gedanken, A. Optimization of sintering on the structural, electrical and dielectric properties of SnO_2 coated $CuFe_2O_4$ nanoparticles. *Materials Chemistry and Phyics* 99 (2006)109-116.

24. Kezzim, A.; Nasrallah, N.; Abdi, A.; Trari, M. Visible light induced hydrogen on the novel hetero-system $CuFe_2O_4$/TiO_2. *Energy Conversion and Management* 52 (2011) 2800-2806.

25. Xiaoxiang, X.; Azad, Abul K.; Irvine, J.T.S. Photocatalytic H_2 generation from spinels $ZnFe_2O_4$, $ZnFeGaO_4$ and $ZnGa_2O_4$. *Catalysis Today* 199 (2013) 22-26.

26. Ragupathi, C.; Judith Vijaya, J.; John Kennedy, L. Preparation, characterization and catalytic properties of nickel aluminate nanoparticles: A comparison between conventional and microwave method. *Journal of Saudi Chemical Society* 21 (2014) S231-S239.

27. Elakkiyaa, V.; Yash, A.; Shanmugam, S. Photocatalytic activity of divalent ion (copper, zinc and magnesium) doped $NiAl_2O_4$. *Solid States Sciences* 82 (2018) 92-98.

28. Lahmar, H.; Kebir, M.; Nasrallah, N.; Trari, M. Photocatalytic reduction of Cr(VI) on the new hetero-system $CuCr_2O_4$/ZnO. *Journal of Molecular Catalysis. A: Chemical* (2012) 74-79.

29. Derbal, A.; Omeiri, S.; Bouguelia, A.; Trari, M.; Characterization of new heterosystem $CuFeO_2$/SnO_2 application to visible-light induced hydrogen evolution.

International Journal of Hydrogen Energy 33, 16 (2008) 4274-4282.

30. Elena Adin, R.; Adina Roxana, P.; Nicoleta Liliana, O.; Cosmina Andreea, L.; Daniela, C.; Maria, M.; Tandem adsorption-photodegradation activity induced by light on NiO-ZnO *p–n* couple modified silica nanomaterials. *Materials Science in Semiconductor Processing journal* 57 (2017) 1-11.

31. Brahimi, R.; Bessekhouad, Y.; Nasrallah, N.; Trari, M. Visible light CrO_4^{2-} reduction using the new $CuAlO_2$/CdS hetero-system. *Journal of Hazardous Materials* 219-220 (2012) 19-25.

32. Chabani, M.; Amrane, A.; Bensmaili, A. Equilibrium sorption isotherms for nitrate on resin Amberlite IRA 400. *Journal of Hazardous Materials* 165 (2009) 27-33.

33. Peng, S.; Jun, Z.; Wenxiu, L.; Qi, W.; Wenbin, C. Modification to L-H Kinetics Model and Its Application in the Investigation on Photodegradation of Gaseous Benzene by Nitrogen-Doped TiO_2. *Catalysts* (2018) 8(8) 326.